

## NEUROSCIENCE

# Genome-wide and phenotype-wide studies provided insights into brain glymphatic system function and its clinical associations

Lusen Ran<sup>1†</sup>, Yuanyuan Fang<sup>1†</sup>, Chang Cheng<sup>1†</sup>, Yuqin He<sup>1</sup>, Zhonghe Shao<sup>2</sup>, Yifan Kong<sup>2</sup>, Hao Huang<sup>1</sup>, Shabei Xu<sup>1</sup>, Xiang Luo<sup>1</sup>, Wei Wang<sup>1\*</sup>, Xingjie Hao<sup>2\*</sup>, Minghuan Wang<sup>1\*</sup>

We applied an MRI technique diffusion tensor imaging along the perivascular space (DTI-ALPS) for assessing glymphatic system (GS) in a genome-wide association study (GWAS) and phenotype-wide association study (PheWAS) of 40,486 European individuals. Exploratory analysis revealed 17 genetic loci significantly associating with the regional DTI-ALPS index. We found 58 genes, including *SPPL2C* and *EFCAB5*, which prioritized in the DTI-ALPS index subtypes and associated with neurodegenerative diseases. PheWAS of 241 traits suggested that body mass index and blood pressure phenotypes closely related to GS function. Moreover, we detected disrupted GS function in 44 of 625 predefined disease conditions. Notably, Mendelian randomization and mediation analysis indicated that lower DTI-ALPS index was a risk factor for ischemic stroke (odds ratio = 1.56,  $P = 0.028$ ) by partly mediating the risk factor of obesity. Results provide insights into the genetic architecture and mechanism for the DTI-ALPS index and highlight its great clinical value, especially in cerebral stroke.

Copyright © 2025 The Authors, some rights reserved; exclusive licensee American Association for the Advancement of Science. No claim to original U.S. Government Works. Distributed under a Creative Commons Attribution NonCommercial License 4.0 (CC BY-NC).

## INTRODUCTION

The glymphatic system (GS) is a brain-wide circulation pathway for the direct exchange of cerebrospinal fluid (CSF) with interstitial fluid (ISF), proceeding from the arterial side to perivenous drainage channels (1). There are numerous reports of GS dysfunction in association with aging and various central nervous system (CNS) diseases, especially neurodegenerative diseases (2–5). Diffusion tensor imaging along the perivascular space (DTI-ALPS) index is a diffusion magnetic resonance imaging (MRI) method that provides an important metric of the anatomic substrate for fluid flow in the GS (6, 7). As a noninvasive method, the DTI-ALPS index is more amenable and common used for clinical application than imaging of intrathecally injected contrast agent to image GS flow, and there is a high correlation between these two metrics (8).

The role of GS function in diseases has attracted extensive attention, and clinical studies generally concur in showing disturbed GS function in CNS diseases such as stroke, multiple sclerosis (MS), cerebral small vessel disease, and Alzheimer's disease (AD) (6, 9–11). To date, there has been no exploration of the association between GS function and risk factors for those diseases, such as sedentary lifestyle and smoking, and there is limited information about GS function in systemic conditions such as diabetes or cardiovascular disease. Moreover, clinical research of the GS function to date mainly used cross-sectional correlation analysis, without detailed investigation of mechanisms and causal inference. Although the expression of several genes (e.g., *SLC13A3*, *WNT7A*, and *EFEMP1*) were related to perivascular space (PVS) (12), there is no large population study for GS function related genes. In addition, there are

discrepancies of the GS function among certain clinical studies. For example, studies of migraine patients include findings of decreased (13), increased (14), and unaffected GS function as compared with controls (15). Such discrepancies may reflect the generally small sample sizes in such clinical investigations.

Aiming to address the limitations of existing clinical studies and comprehensively explore the genetic, phenotypic factors and causal relationship related to the GS, we evaluated GS function according to the modified DTI-ALPS index, and identified genetic loci among nearly 40,000 individuals. We also explored the relationship between DTI-ALPS index and hundreds of phenotypes, including more than 200 potential traits and more than 600 systemic diseases. Last, we used Mendelian randomization models to examine the causal and mediating role of the GS function, focusing on obesity and stroke.

## RESULTS

### Overview of study

We first evaluated the GS function by diffusion MRI data from the UK Biobank, which yielded 40,486 sets of DTI-ALPS index data, including the anterior (aALPS), middle (mALPS), posterior (pALPS), total DTI-ALPS (tALPS) indices (Fig. 1A; details in Materials and Methods). We found that DTI-ALPS index of males was significantly lower than females (1.35 versus 1.50,  $P < 0.001$  for tALPS) (fig. S1A). Overall, the DTI-ALPS index decreased with increasing age ( $\beta = -0.077$ ,  $P < 0.001$  for tALPS) and there may exist slightly differences between the decline rates of males and females (table S1 and fig. S1B). We then performed genome-wide association study (GWAS) of these DTI-ALPS index in 31,629 unrelated individuals of European ancestry with 14,611,868 single-nucleotide polymorphisms (SNPs) (Fig. 1B). We next performed the phenotype-wide association study (PheWAS) of DTI-ALPS index with 866 phenotypes, comprising eight categories of traits and 12 systemic diseases (Fig. 1C). Last, we used Mendelian randomization and mediation analysis models to examine the roles of DTI-ALPS index in obesity and stroke (Fig. 1D).

<sup>1</sup>Department of Neurology, Tongji Hospital, Tongji Medical College, Huazhong University of Science and Technology, Wuhan, China. <sup>2</sup>Department of Epidemiology and Biostatistics, Ministry of Education Key Laboratory of Environment and Health, School of Public Health, Tongji Medical College, Huazhong University of Science and Technology, Wuhan, China.

\*Corresponding author. Email: mhwang@tjh.tjmu.edu.cn (M.W.); xingjie@hust.edu.cn (X.H.); wwang@vip.126.com (W.W.)

†These authors contributed equally to this work.

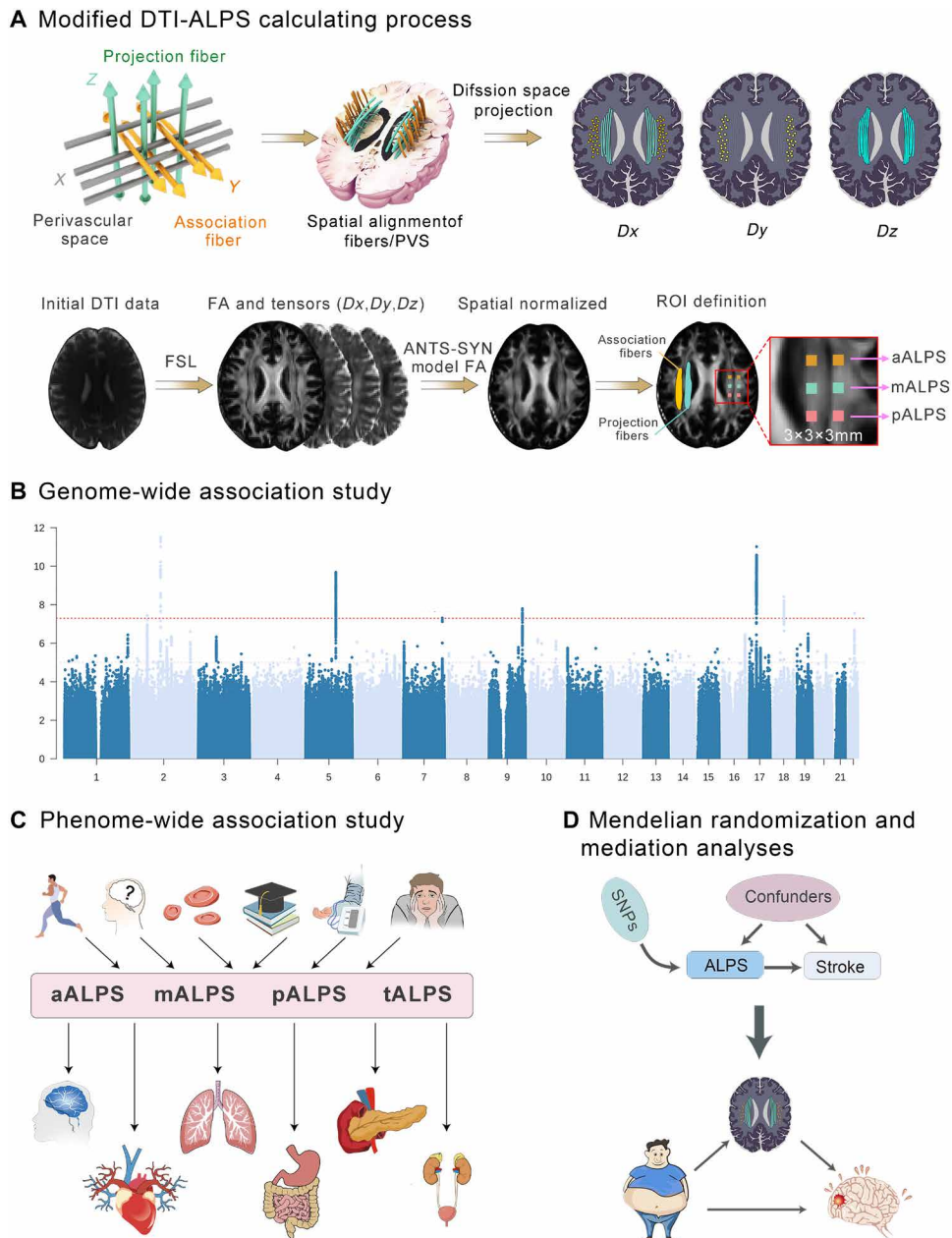


**Fig. 1. Modified DTI-ALPS index calculation process and full-text flow chart.** Tensor imaging  $D_x$  quantifies the diffusion of water molecules along the PVS of the medullary vein in projection and association white matter fiber regions; tensor imaging  $D_y$  quantifies free diffusion in projective fiber regions; tensor imaging  $D_z$  quantifies free diffusion in association fiber regions. We calculated the individual FA and tensors ( $D_x$ ,  $D_y$ , and  $D_z$ ) in the source DTI data and registered them to the standard space. We placed  $3 \times 3 \times 3$  mm ROIs in association and projection fibers in the FA imaging. The signal intensity values from the individual regressed tensors in each ROI were taken to calculate aALPS, mALPS, and pALPS, and their average, tALPS (A). We first undertook the GWAS analysis to find SNPs with significant association with the DTI-ALPS index (B). We next explored the phenome-wide observational association study of traits and diseases related to the DTI-ALPS index in the UK Biobank (C). We then took the Mendelian randomization model to establish the causal relationship between DTI-ALPS index and obesity and stroke, and lastly analyzed the mediating effect of ALPS on stroke in association with obesity (D).

### GWAS of the GS function

We carried out GWAS for GS function evaluated by each of the four DTI-ALPS indexes after standardized and stringent quality controls (details in Materials and Methods). We successfully identified 17 significant loci ( $P < 5 \times 10^{-8}$ ), including eight for aALPS, four for mALPS, three for pALPS, and five for tALPS (Fig. 2, A, C, E, and G, and Table 1).

The intercepts of the linkage disequilibrium (LD) score regression (LDSC) ranged from 1.013 to 1.024 (fig. S2), indicating that the population structure was well controlled and that the inflation was mostly due to polygenicity (16). In addition, the LDSC estimates of SNP heritability ranged from 0.231 (mALPS) to 0.243 (tALPS) (table S2), suggesting that the GS function was well influenced by genetic factors.

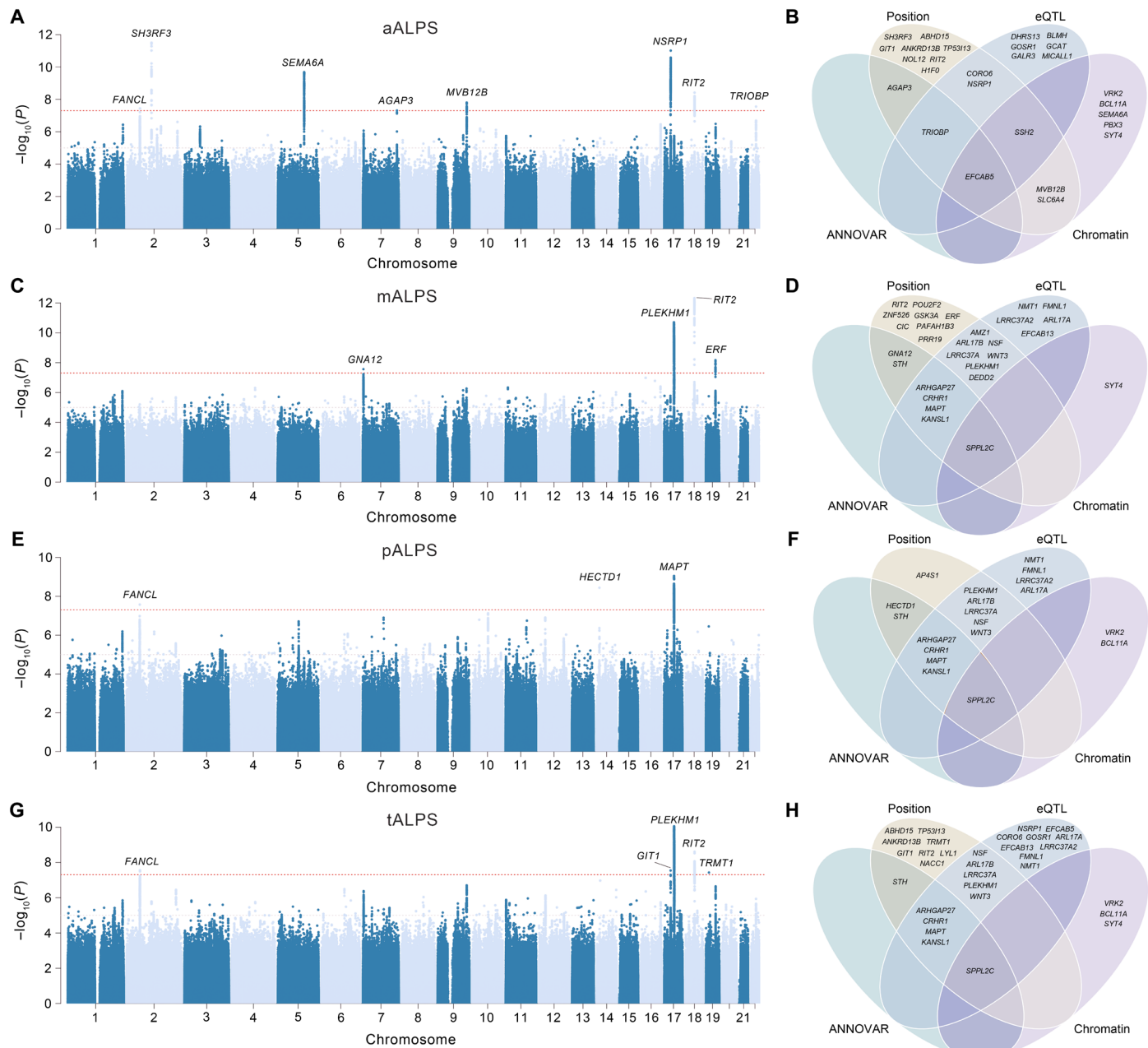


**Fig. 2. Manhattan and Venn diagram plots of DTI-ALPS index.** Manhattan plots of the GWASs of (A) aALPS, (C) mALPS, (E) pALPS, and (G) tALPS. The red dash line indicates the genome-wide significance level of  $5 \times 10^{-8}$ . The closest protein-coding gene for the lead variant in each locus was labeled. Venn plots of mapped genes by four gene prioritization approaches for (B) aALPS, (D) mALPS, (F) pALPS, and (H) tALPS.

To obtain an insight into the functional consequences of genetic variants associated with DTI-ALPS index, we used the Functional Mapping and Annotation (FUMA) platform to annotate the associated loci. Functional annotations of these SNPs at the associated loci were mainly located in intronic, intergenic, and noncoding RNA intronic areas (fig. S3). In addition, by using four approaches (ANNOVAR, positional mapping, eQTL mapping, and chromatin interaction mapping; details in Materials and Methods), we prioritized 58 genes for the four DTI-ALPS indexes, namely, 27 genes for aALPS, 28 for mALPS, 19 for pALPS, and 31 for tALPS (Fig. 2, B, D,

F, and H). For example, we prioritized genes due to nonsynonymous mutations at 17q21.31, including *ARHGAP27*, *CRHR1*, *SPPL2C*, *MAPT*, *STH*, and *KANSL1*, which are associated with schizophrenia and brain structure (17) (table S3). Notably, *EFCAB5* and *SPPL2C* were prioritized by four approaches in at least one of ALPS regional subtypes. *EFCAB5* at 17q11.2 was implicated by eQTL in brain regions and was mapped in the dorsolateral prefrontal cortex and neural progenitor cells based on chromatin interactions. *SPPL2C* at 17q21.31 was mapped by three DTI-ALPS index (fig. S4) with chromatin interactions in neural progenitor cells and was implicated by

**Table 1. Details of the lead SNPs for each locus for GWAS of the DTI-ALPS index.** GWAS, genome wide association study; DTI-ALPS, diffusion tensor imaging along the perivascular space; aALPS, anterior DTI-ALPS index; mALPS, middle DTI-ALPS index; pALPS, posterior DTI-ALPS index; tALPS, total DTI-ALPS index; SNPs, single-nucleotide polymorphisms; CHR, chromosome; BP, base pair position; EAF, effect allele frequency; EA/NEA, effect allele/non effect allele.

SNP	CHR	BP	Gene	EA/NEA	EAF	$\beta$	SE	P
<b>aALPS</b>								
rs62140788	2	58,685,657	<i>FANCL</i>	G/C	0.18	0.010	0.0019	$3.6 \times 10^{-8}$
rs4676274	2	109,948,720	<i>SH3RF3</i>	T/C	0.49	0.010	0.0015	$3.1 \times 10^{-12}$
rs1845561	5	116,621,378	<i>SEMA6A</i>	A/G	0.34	-0.010	0.0016	$2.1 \times 10^{-10}$
rs59089786	7	150,806,326	<i>AGAP3</i>	TA/T	0.32	0.009	0.0016	$4.9 \times 10^{-8}$
rs7028698	9	129,101,518	<i>MVB12B</i>	A/G	0.17	0.011	0.0019	$1.6 \times 10^{-8}$
17:28489042_CT_C	17	28,489,042	<i>NSRP1</i>	C/CT	0.49	-0.010	0.0015	$9.6 \times 10^{-12}$
<b>mALPS</b>								
rs798518	7	2,777,825	<i>GNA12</i>	G/A	0.31	-0.010	0.0019	$2.7 \times 10^{-8}$
rs1879582	17	43,570,680	<i>PLEKHM1</i>	T/C	0.18	-0.015	0.0022	$2.0 \times 10^{-11}$
rs9961058	18	40,273,285	<i>RIT2</i>	T/C	0.26	-0.014	0.0020	$4.8 \times 10^{-13}$
rs57938324	19	42,764,352	<i>ERF</i>	C/T	0.06	-0.021	0.0036	$6.8 \times 10^{-9}$
<b>pALPS</b>								
rs2215939	2	58,719,447	<i>FANCL</i>	T/A	0.35	0.008	0.0016	$2.7 \times 10^{-8}$
rs61976859	14	31,583,512	<i>HECTD1</i>	T/C	0.10	-0.014	0.0024	$3.6 \times 10^{-9}$
rs2435204	17	43,988,205	<i>MAPT</i>	G/A	0.23	-0.011	0.0018	$8.9 \times 10^{-10}$
<b>tALPS</b>								
rs2215939	2	58,719,447	<i>FANCL</i>	T/A	0.35	0.008	0.0015	$2.8 \times 10^{-8}$
rs72624990	17	27,916,776	<i>GIT1</i>	C/G	0.40	-0.008	0.0014	$2.9 \times 10^{-8}$
rs375822897	17	43,557,054	<i>PLEKHM1</i>	AAAAA-CAAAAC/A	0.17	-0.012	0.0018	$9.0 \times 10^{-11}$
rs652050	18	40,201,177	<i>RIT2</i>	A/G	0.28	-0.009	0.0015	$2.5 \times 10^{-9}$
rs35601737	19	13,220,703	<i>TRMT1</i>	G/C	0.31	0.008	0.0015	$3.8 \times 10^{-8}$

eQTL in the cerebellar hemispheres, entire cerebellum, and cerebral cortex. Moreover, by lookup scrutiny of the GWAS catalog, we found that many of the significant SNPs of our study were also associated with white matter microstructure and other brain structural measures, the neuroticism trait, neuropsychiatric disorders, sleep disorders, and neurodegenerative diseases.

#### PheWAS of GS function for traits

We first investigated the associations between 241 traits covering eight fields with GS function evaluated by DTI-ALPS index, which yielded 128 traits with significant associations with DTI-ALPS index after correction for multiple testing ( $P < 2.07 \times 10^{-4}$ ; details in Materials and Methods; Fig. 3). Among these, 87 traits were associated with four regional subtypes of the DTI-ALPS index. Traits related to obesity (such as waist-to-hip ratio, leg fat percentage, and body fat percentage), high blood pressure and elevated pulse rate, smoking (heavy smoking, cigarettes smoked per year, and current smoking), reticulocyte count and percentage, habitual napping, snoring, time spent watching television, and computer activity emerged as risk factors. Conversely, brisk walking pace, good lung function [such as forced expiratory volume in 1 s (FEV1), forced vital capacity (FVC)], physical activity [PA; high PA level, PA days,

and sum metabolic equivalent of task (MET) of PA], lesser facial aging, sometimes or often alcohol consumption, and good cognitive function were protective factors.

A number of variables specifically influenced a domain of DTI-ALPS index. For example, tower rearranging related only to aALPS increase ( $\beta = 0.002$  and  $P = 8.29 \times 10^{-7}$ ), and minimum intima-media thickness and seated height, was associated with aALPS decrease ( $\beta = -3.74 \times 10^{-5}$ ,  $P = 5.82 \times 10^{-5}$ ; and  $\beta = -0.001$ ,  $P = 1.60 \times 10^{-4}$ ). Time outdoors in winter and dried fruit consumption were only associated with mALPS increase ( $\beta = 0.003$ ,  $P = 1.19 \times 10^{-4}$ ; and  $\beta = 0.002$ ,  $P = 1.54 \times 10^{-4}$ ) and medium income related to mALPS decrease ( $\beta = -0.010$ ,  $P = 8.83 \times 10^{-5}$ ). Lamb consumption was associated only with tALPS increase ( $\beta = 0.009$ ,  $P = 8.56 \times 10^{-5}$ ) and other alcohol intake weekly and occasional current smoking related to tALPS decrease ( $\beta = -0.009$ ,  $P = 1.95 \times 10^{-4}$ ; and  $\beta = -0.028$ ,  $P = 1.83 \times 10^{-4}$ ).

#### PheWAS of GS function for diseases

Our PheWAS of GS function evaluated by each DTI-ALPS index with 625 system-wide diseases have yielded 44 diseases showing significant associations with decreased DTI-ALPS index (Details in method, Fig. 4). Thirty diseases were associated with aALPS, including

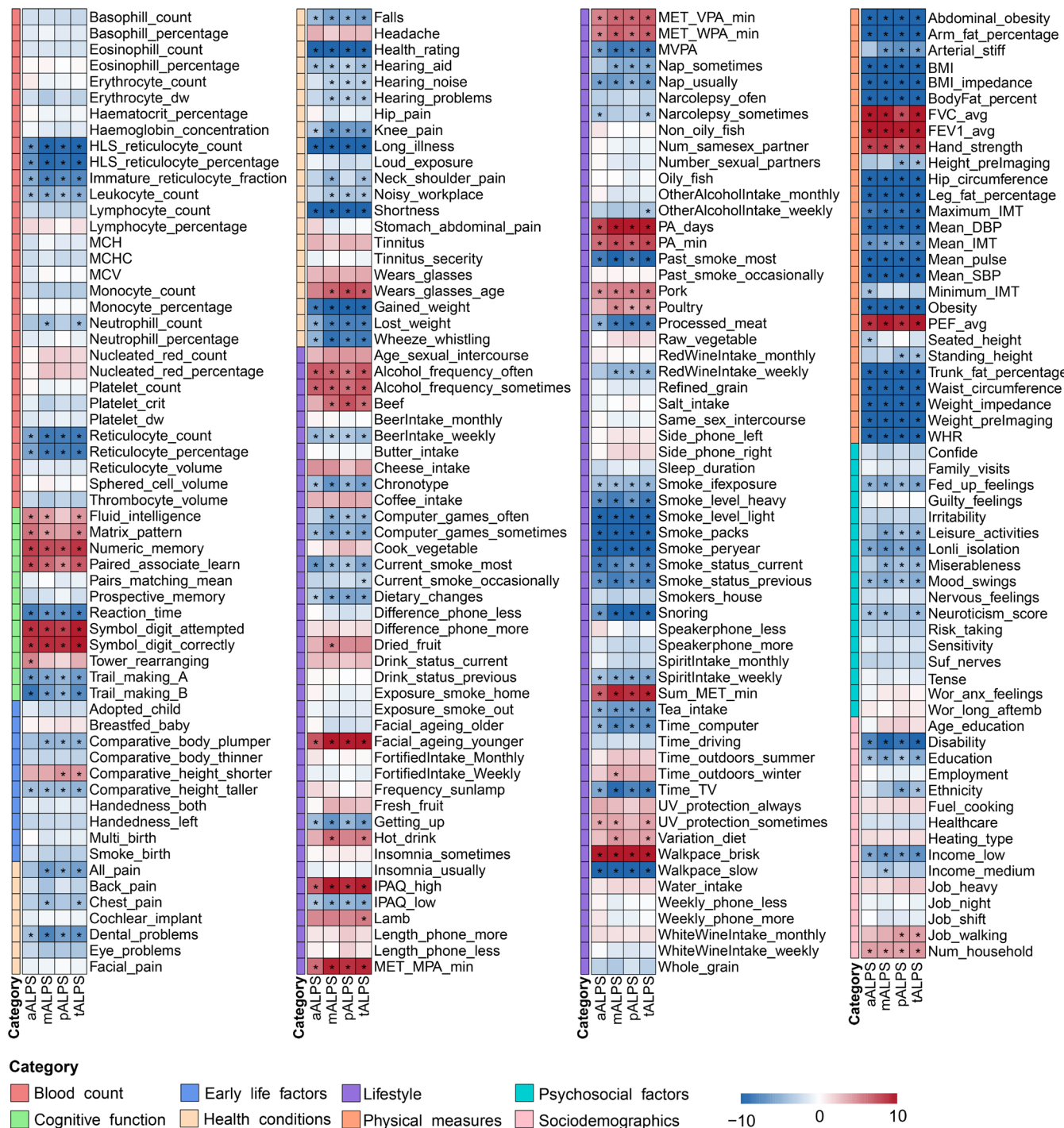


**Fig. 3. PheWAS of DTI-ALPS index with related traits.** We selected 241 variables covering nine fields (sociodemographic, lifestyle, early life factors, psychosocial factors, health conditions, physical measures, cognitive function, and blood count) to explore the traits of each DTI-ALPS index. Blue represents negative correlation and red represents positive correlation. Adjustment for sex, age, and Townsend deprivation index. \* indicates the items that were significant after Bonferroni correction ( $P < 2.07 \times 10^{-4}$ ).

six cardiovascular diseases, five endocrine diseases, and three nervous systems. Cerebral infarction ( $\beta = -0.08, P = 3.07 \times 10^{-8}$ ), MS ( $\beta = -0.08, P = 2.73 \times 10^{-7}$ ), and other cerebrovascular diseases ( $\beta = -0.07, P = 2.98 \times 10^{-5}$ ) had the largest effect on aALPS (Fig. 4A). Thirty-nine diseases were associated with mALPS, including seven cardiovascular diseases, six endocrine diseases, and

five nervous system diseases. Among these diseases, Parkinson's disease (PD;  $\beta = -0.10, P = 3.41 \times 10^{-5}$ ) and type 1 diabetes ( $\beta = -0.10, P = 2.11 \times 10^{-8}$ ) had the largest effect on mALPS (Fig. 4B). Thirty diseases were associated with pALPS, including six cardiovascular diseases, six endocrine diseases, and two nervous system diseases. Among these, MS ( $\beta = -0.10, P = 9.53 \times 10^{-12}$ ), type



**Fig. 4. PheWAS of DTI-ALPS index with diseases.** PWAS results of aALPS (A), mALPS (B), pALPS (C), and tALPS (D) index. The  $-\log_{10}$  of association  $P$  values were displayed using the Manhattan plot, and the effect sizes of significant associations were displayed using the forest plot. The color indicates different disease categories. The plots above the dotted line represent  $P$  values that were significant after Bonferroni correction adjusting for 635 diseases ( $P < 8.00 \times 10^{-5}$ ).

1 diabetes ( $\beta = -0.08, P = 1.29 \times 10^{-8}$ ), and unspecified diabetes ( $\beta = -1.14, P = 2.98 \times 10^{-42}$ ) had the largest effect on pALPS (Fig. 4C). Forty-one diseases were associated with tALPS, including eight cardiovascular diseases, seven endocrine diseases, and four nervous system diseases. Among these, MS ( $\beta = -0.10, P = 1.25 \times 10^{-12}$ ), hemiplegia ( $\beta = -0.09, P = 3.81 \times 10^{-5}$ ), and type 1 diabetes ( $\beta = -0.08, P = 1.43 \times 10^{-8}$ ) had the largest effect on tALPS (Fig. 4D).

### Mendelian randomization and mediation study of obesity, GS function, and stroke

Previous studies have observed the GS function decline related to stroke, but without a clear causal relationship of them. To probe in-depth the possible causal relationship between GS function and stroke, we performed a bidirectional Mendelian randomization analysis. When taking GS function evaluated by DTI-ALPS index as exposure and stroke subtypes as outcome, tALPS emerged as a protective factor with total stroke (ischemic or hemorrhagic) [odds ratio (OR) = 0.67,  $P = 0.033$ ] and ischemic stroke (OR = 0.64,  $P = 0.028$ ) (Fig. 5A). The causal relationships remained when taking small vessel stroke as exposure and tALPS as outcome ( $\beta = -0.01, P = 0.030$ ) (fig. S5). When taking obesity indicators as the exposure and tALPS as outcome, Mendelian randomization analysis supported the conclusion that obesity was a risk factor for tALPS, specifically for indicators of body mass index (BMI) ( $\beta = -0.02, P = 0.002$ ), body fat mass ( $\beta = -0.04, P < 0.001$ ), body fat percentage ( $\beta = -0.05, P < 0.001$ ), and body fat measures at trunk, arm, and leg (Fig. 5B). As positive control, we verified the causality between obesity and stroke, with all measures of obesity as a cause of stroke, regardless of whether outcome was total stroke or ischemic stroke (Fig. 5C and fig. S6).

On the basis of the Mendelian randomization analysis results, we calculated the mediating role of tALPS in obesity-induced ischemic stroke (Fig. 5D). The tALPS had a significant mediating effect on adiposity measured by body fat mass (indirect effect = 0.016,  $P = 0.045$ ), body fat percentage (indirect effect = 0.021,  $P = 0.047$ ), and trunk fat mass (indirect effect = 0.016,  $P = 0.045$ ). The mediation percentages for them were 10.1, 9.8, and 10.7% respectively. For details of the other relevant mediation analysis results, see table S4 to S9.

### DISCUSSION

In this first large-scale population GWAS and PheWAS study of GS function, we identified 17 loci associated with the GS function and showed associations of GS function with cardiovascular-related phenotypes and various systemic diseases. Specifically, we illustrated that lower DTI-ALPS index was a risk factor of stroke by partly mediating the risk factor of obesity.

Through comprehensive functional annotation of linked genetic variants, we revealed that the genetic component of GS function was associated mainly with neurodegenerative diseases. A notable example is *RIT2*, with the strongest SNP signal at 18q12.3 (rs9961058), encoding a neuronal guanosine triphosphatase (GTPase), which can modulate dopaminergic signaling by interacting directly with the plasma membrane dopamine transporter (DAT) (18). Using four gene prioritization approaches, we identified *EFCAB5* and *SPPL2C* as the candidate genes. *EFCAB5* is involved in various nervous system processes, which can affect synapse formation and maturation, as well as dendritic growth and branching (19). *EFCAB5* is also

implicated in brain aging in previous studies (20, 21). *SPPL2C* encodes a catalytically active GxGD-type intramembrane aspartyl protease, which has emerged as a key factor driving pathologies in AD (22). In addition, previous studies have shown that a nonsynonymous mutation (rs12373123) in *SPPL2C* associated with AD can affect the expression of *GRN* in microglia and *MAPT* in astrocytes, these being key genes in frontotemporal dementia and PD (23). All these genetic findings were further indicated a link between GS function and neurodegenerative diseases. Previous animal experiments and clinical studies have confirmed that the GS is involved in the occurrence and progression of neurodegenerative diseases by virtue of its role in the elimination of neurotoxic protein aggregations such as amyloid- $\beta$  and tau in AD and  $\alpha$ -synuclein in PD (24–26). This study is the first to establish the genetic association between the GS and neurodegenerative diseases, thereby offering a fresh perspective for future research in this field.

From the genetic point of view, DTI-ALPS is closely related to neurodegenerative diseases. In our PheWAS results, we found that PD was associated with mALPS ( $\beta = -0.10, P = 3.41 \times 10^{-5}$ ). We could not include other typical neurodegenerative diseases like AD in our PheWAS because of their low prevalence (one or two cases). We excluded diseases in the bottom 10% of prevalence among the 791 diseases specified in the UK Biobank, because their analysis would have introduced large biases. Previous clinical reports about the DTI-ALPS index in AD showed that the DTI-ALPS score closely correlated with MMSE score (6, 7, 27). Other prior reports showed that DTI-ALPS in early-onset AD correlated with volumes of cortical and subcortical structures (28). Case-control studies found a decrease in DTI-ALPS in patients with PD and revealed that DTI-ALPS correlated with severity of movement disorders (29, 30). Thus, a range of studies have related dysfunction of the GS to the severity of neurodegenerative diseases and their symptoms.

In this first large-scale, population-based study of the GS, we identified a diverse array of traits from eight domains: sociodemographic, lifestyle, early life factors, psychosocial factors, health conditions, physical measures, cognitive function, and blood cell counts. We found several key physiological regulators, including respiratory function (31), high blood pressure and pulse rate (which relate to cardiovascular pulsatility) (32–34), voluntary exercise/physical activity (35, 36), and indicators related to obesity, such as waist-to-hip ratio and BMI can influence GS function. Besides, body fat percentage showed a close association with MRI-ALPS indices of GS function. Furthermore, we also observed that good cognitive function was associated with robust GS metrics, thus confirming a previous study (6). Animal experiments and analogous studies in humans demonstrate the dependence of GS on sleep state, and sleep deprivation interferes in the clearance of metabolic waste clearance (37, 38). Our analyses revealed snoring to be a risk factor for GS impairment, which was consistent with a recent study indicating that continuous positive airway pressure increases CSF flow and GS transport (39). We first identified relatively unexplored factors, including smoking and alcohol use frequency, walking pace, facial aging, and reticular count and percentage. We speculate that insofar as smoking certainly causes atherosclerosis, and reticulocytosis affects cerebral blood flow, the net result is declining GS function. Brisk walking pace predicts good body and brain health (40) and facial aging is a conspicuous manifestation of aging (41), which may indicate good GS function. Whereas even moderate alcohol consumption accelerates brain aging (42), our analysis found that the

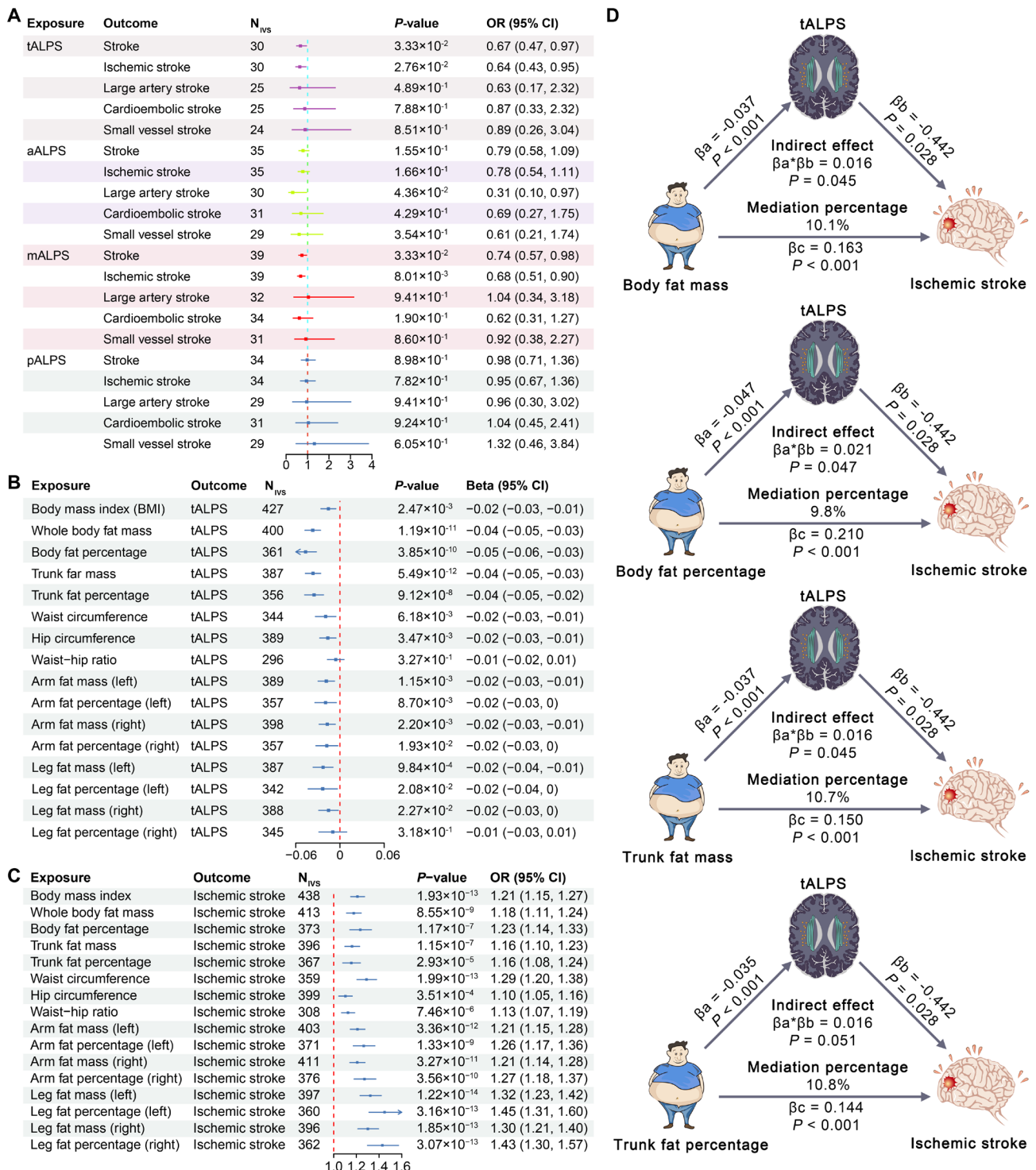


**Fig. 5. Mendelian randomization analysis of the role of DTI-ALPS index in obesity indicators and stroke subclasses.** Two-sample Mendelian randomization analysis results (IVW model) for DTI-ALPS index to stroke (A), obesity to tALPS (B), and obesity to ischemic stroke (C). OR was presented for the outcome of stroke, and  $\beta$  value was presented for the outcome of DTI-ALPS index. On the basis of the Mendelian randomization analysis results, tALPS had a significant mediating effect on obesity-caused ischemic stroke measured by body fat mass, body fat percentage, and trunk fat mass (D). The P values presented are all original.

regular or occasional alcohol consumption was associated with good GS, which calls for independent confirmation. Thus, our study provides novel insights into the factors influencing GS function with solid human clinical evidence corresponding to previous experimental animal studies, with a robustness derived from the large sample size in the UK Biobank.

Our study also includes broad coverage of systemic diseases in relation to GS function. The spectrum covers common diseases in every organ system, standardized according to the ICD-10 classification. Although previous reports have found association of GS with MS, strokes, and diabetes (10, 11, 43, 44), present results further emphasize the strong association of these disorders with GS dysfunction. We also find that GS integrity has close associations with systemic diseases outside the CNS, which has scant documentation in the previous GS literature. Regarding cardiovascular disease, we found that hypertension, atrial fibrillation, and angina were associated with decreased GS function. These three conditions are commonly detrimental to pulsation of the cerebral arteries, which is a key driver for ISF/CSF exchange via the GS (45). Respiratory diseases such as chronic obstructive pulmonary disease and asthma also displayed associations with decreased GS function. The CNS is notoriously dependent on blood oxygen delivery, and long-term chronic hypoxia is associated with dementia and cognitive decline (46, 47). Unexpectedly, we found associations between declining GS function with diseases of the extended digestive system including liver disease, gallbladder disease, esophagitis, and abdominal hernia. The emerging concept of the gut-brain proposes a close relationship between the digestive system and CNS health (48). These associations entail regulation of intestinal flora and immune cells in reciprocal interaction with the brain (49–51), but a particular mechanism for association between the digestive system and GS function remains to be established.

Mendelian randomization analysis indicated a causal relationship between obesity and GS function. In a previous clinical study, Wei *et al.* (52) showed that excessive BMI and waist circumference were associated with decreased GS function, but did not include direct measures of body fat in their analyses. Our Mendelian randomization further indicated that obesity, especially as body fat metrics, was a driver for declining GS function. Although the pathway for this relationship is unspecified, we speculate that GM failure follows upon the vascular dysfunction due to obesity-related metabolic syndrome. Whereas previous studies have focused on the functional changes of GS after stroke, present results identified reduced GS function as a cause of stroke. Insofar as the main function of the GS is to clear metabolic waste from brain, GS impairment may cause cerebrovascular dysfunction (53), leading to increased stroke risk. These results may imply a feed forward mechanism where GS dysfunction and stroke form a vicious circle of neurological impairment. We further propose a mechanism whereby GS dysfunction is a factor out mediation model of obesity-induced stroke. As distinct from a traditional mediation analysis model, our analysis entails Mendelian randomization, which makes our results more robust by introducing genetic factors in the pathway from obesity to GS dysfunction to stroke. That GS function may be among the predictors of stroke in obese patients enhances the clinical value of DTI-ALPS.

Preclinical studies have found that the glymphatic pathway has region-specific differences in clearance rates (25, 54, 55). Therefore, referring to the approach of Jiang *et al.* (56), we made an anatomic segmentation of the DTI-ALPS index into three regions (aALPS,

mALPS, and pALPS) and their aggregate tALPS) (details in Materials and Methods). In an exploratory analysis of functional correlates, we found that performance of the tower rearranging cognitive test was only associated with aALPS, which contains fibers arising from the frontal cortex projecting in the anterior corona radiata. Notably, the tower rearranging task largely reflects the executive function of the frontal cortex (57, 58). In contrast, hyperthyroidism was only associated with tALPS, consistent with a global cerebral manifestation of a disorder affecting metabolism throughout the body. PD was only associated with mALPS, which contains the superior thalamic radiation, thus likely capturing a disturbance of the cortico-striato-thalamo-cortical loop that plays a crucial role in PD (59, 60). Results of the present brain-wide exploration of DTI-ALPS relation to specific disease conditions should set the stage for prospective studies of the functional consequences of regional DTI-ALPS changes.

It is worth noting that the DTI-ALPS index more represents tissue pathology than a tool for the direct measure of GS function per se. The initiators of the DTI-ALPS method emphasize that it is an imaging marker of a structural correlate of GS function (61, 62). Although DTI-ALPS is currently the most widely used GS measurement in clinical research, we see a need for developing more direct and comprehensive methods for measuring GS function directly to verify the conclusions drawn in this study (62).

Our study has several limitations. First, most of the UK Biobank participants are of European ethnicity populations, so it remains to be seen if results will generalize to other databases. Second, DTI-ALPS index is the most widely used and verified index of GS function in clinical practice, but does not directly measure GS function as assessed by the gold standard method of intrathecal contrast imaging. Last, although we focused on the relationships between GS function and obesity and stroke, many genetic factors and other diseases evidently had a relation to GS function. Other positive results found in the association analysis are worthy of further mechanistic exploration.

## MATERIALS AND METHODS

### Imaging and phenotype and data source

The UK Biobank is a large-scale prospective study that enrolled over 500,000 individuals aged 40 to 69 from 22 assessment centers between 2006 and 2010. The UK Biobank has received ethical approval from MREC (reference: 11/NW/0382) and written informed consent was provided by all participants.

After the release of brain imaging data of approximately 40,000 participants in early 2020 (63), we acquired the diffusion MRI data for our main analysis. After excluding incomplete datasets or unusefully blurred images, we used the diffusion MRI data from 40,486 participants of mean age  $64.0 \pm 7.7$  years (range, 45 to 82 years). There were 19,026 (47%) males, of mean age  $46.7 \pm 7.8$  years, and the females were of mean age  $63.4 \pm 7.5$  years. The brain MRI data were all acquired on a single Siemens Skyra 3-T scanner. The sequence parameters of diffusion MRI are available at [https://biobank.ctsu.ox.ac.uk/crystal/crystal/docs/brain\\_mri.pdf](https://biobank.ctsu.ox.ac.uk/crystal/crystal/docs/brain_mri.pdf). We used the brain diffusion MRI data from the “40k” (approximately 40,000 participants). The diffusion MRI data were preprocessed and analyzed by the UK Biobank brain imaging team using FMRIB Software Library (FSL) tools (<https://fsl.fmrib.ox.ac.uk/fsl/docs/#/>).

Consenting participants also provided regular blood, urine, and saliva samples, as well as detailed personal information, to enable an

in-depth assessment of genetic and health factors. We recorded 241 traits of participants at the time of their first MRI. These traits are grouped into eight categories: sociodemographic, lifestyle, early life factors, psychosocial factors, health conditions, physical measures, cognitive function, and blood cell counts. We also obtained the disease diagnosis of participants at the time of the first MRI according to the categories that “first occurrence” in the UK Biobank. There were 791 diseases included, among which 625 were eventually selected for subsequent analysis after excluding those in the bottom 10% of prevalence. These diseases involve 12 major systems of the body: infectious and parasitic diseases, blood, blood-forming organs and certain immune disorders, endocrine, nutritional and metabolic diseases, mental and behavioral disorders, nervous system disorders, circulatory system disorders, respiratory system disorders, digestive system disorders, genitourinary system disorders, skin and subcutaneous tissue disorders, musculoskeletal system and connective tissue disorders, pregnancy, childbirth, and the puerperium.

### Derivation of imaging phenotypes

We calculated the DTI-ALPS index to assess the glymphatic function as previously described (8, 27, 56). First, we preprocessed DTI data (UK Biobank field ID: 20250) with the FMRIB Software Library (FSL, version 6.0), including denoise, Gibbs unringing, top-up distortion correction, eddy current correction, and N4 bias field correction. Then, we calculated the fractional anisotropy (FA) image and corresponding diffusion tensor images in the  $x$ ,  $y$ , and  $z$  directions ( $D_x$ ,  $D_y$ , and  $D_z$ ) for  $b$  value = 1000 s/mm<sup>2</sup>. Next, we transformed the individual FA images to the FA template of the Johns Hopkins University Diffusion Tensor Imaging atlas (JHU DTI atlas) using Advanced Normalization Tools Symmetric Image Normalization (ANTS-SY) (<https://github.com/ANTsX/ANTs/wiki/Warp-and-reorient-a-diffusion-tensor-image>) (64), and the resultant registration matrix was used for transformation of the individual tensor images. We placed a set of  $3 \times 3 \times 3$  mm region of interests (ROIs) in the anterior, middle, and posterior regions of the association and projection fibers from the FA template (JHU DTI atlas) manually. Last, this set of ROIs was used in all spatial normalized FA and tensors to calculate DTI-ALPS index of all the individuals. We extracted the  $x$ -axis diffusivity ( $D_{x\text{proj}}$ ) and  $y$ -axis diffusivity ( $D_{y\text{proj}}$ ) of ROIs in the projection fibers, and  $x$ -axis diffusivity ( $D_{x\text{assoc}}$ ) and  $z$ -axis diffusivity ( $D_{z\text{assoc}}$ ) of ROIs in the association fibers. The DTI-ALPS index is defined as [mean ( $D_{x\text{proj}}$ ,  $D_{x\text{assoc}}$ )]/[mean ( $D_{y\text{proj}}$ ,  $D_{z\text{assoc}}$ )], being classified as aALPS, mALPS, and pALPS according to the spatial location of the fibers. tALPS is defined as the mean of the three preceding indices (Fig. 1, A and B). We randomly sampled 400 cases and checked the accuracy of the ROIs positions, finding in each case a good placement of the ROIs on the projection and association fibers.

For quality control, we first excluded the individuals with missing ( $n = 1974$ ) or poor-quality ( $n = 18$ ) primary imaging files. Second, we counted the FA values of the ROI regions where ALPS was calculated and found that the FA values for all the subjects were greater than 0.3. Last, to compare the effects of the ROI location and size on the results, we made additional analyses in a random selection of 735 individuals. Correlation analysis of DTI-ALPS results in the standard  $3 \times 3 \times 3$  mm ROIs with positionally untranslated  $2 \times 2 \times 2$  and  $4 \times 4 \times 4$  mm ROIs and a positional translated  $3 \times 3 \times 3$  mm ROI indicated consistently excellent agreement (Pearson correlation coefficients from 0.976 to 0.998), and regression

slopes close to unity (fig. S7). Therefore, the dimension and position of ROIs in the white matter region had little effect on precision and accuracy of the results.

### UK Biobank genotyping and quality control

Details of the sample processing, genotyping and quality control have been described elsewhere (65). As in our previous work (66), we focused on the imputed genotypes for the subset of individuals of European ancestry subset, comprising 408,812 samples who self-identified as white British and had very similar genetic ancestry based on the principal component analysis. The variants with minor allele frequency (MAF) <0.001, Hardy–Weinberg equilibrium test  $P$  value < $1.0 \times 10^{-12}$ , missing genotype rate >0.05, number of alleles >2, or imputation accuracy score <0.6 were excluded by using PLINK (67). Last, we retained 408,791 European ancestry individuals and 14,611,868 variants on GRCh37 for the study.

### ALPS GWAS in the UK Biobank

We restricted our GWAS to the population with self-declared European ancestry. After randomly excluding individuals with diseases confounding the cerebral white matter findings (brain trauma, stroke, tumor, MS, etc.) and in related pairs with kinship coefficient  $\geq 0.0884$  (second degree or greater), the ALPS GWASs were conducted in 31,629 individuals by PLINK (67) with a linear regression model adjusting for age, sex, systolic blood pressure, array batch, and top ten ancestry principal components.

### LD score regression

The LDSC (16) was applied to estimate the SNP-based heritability and check the potential effect of population structure. The LD scores were calculated on the basis of the genotypes of European in the 1000 Genomes Project (68) and downloaded from <https://alkesgroup.broadinstitute.org/LDSCORE/>. We only used the GWAS summary statistics of HapMap3 SNPs and further removed the SNPs in the MHC region.

### Gene annotation

We used FUMA version 1.5.2 (<https://fuma.ctglab.nl/>) to identify genomic loci and determine functional consequences of candidate variants in these loci (69). FUMA is an online platform for annotating, prioritizing, visualizing, and interpreting GWAS results by integrating comprehensive annotation data sources. We first identified independent significant SNPs that reached genome-wide significance ( $P < 5 \times 10^{-8}$ ) and were independent of each other by the criterion of  $r^2 < 0.6$ . In a second clumping procedure, these SNPs were further labelled as lead SNPs if they were independent from each other at  $r^2 < 0.1$ . LD blocks of independent significant SNPs within a 1000 kb distance were merged into a single genomic locus (the LD structure was based on the European population of the UKB). All variants with  $r^2 \geq 0.6$ , GWAS  $P$  value < $1 \times 10^{-5}$ , and MAF >0.001 were defined as candidate variants for further annotation. We used four approaches to perform functional annotation and gene mapping by FUMA, including ANNOVAR (“gene-based annotation”) (70), positional mapping, eQTL mapping, and chromatin interaction mapping. Our approach employed ANNOVAR to annotate each SNP according to its genic position, i.e., exon, intron, or intergenic regions. We focused on the genes corresponding to nonsynonymous mutations in exons. Gene mapping was based on Ensembl protein coding genes (version 110). For the

positional mapping of SNPs to genes, we set a maximal distance of 10 kb, based on known protein-coding genes in the human reference assembly (GRCh37). For the eQTL mapping, all candidate SNPs were mapped to eQTLs in the brain tissue samples in GTEx version 8 (71) with the default settings of false discovery rate (FDR) < 0.05 or  $P$  value  $< 1 \times 10^{-3}$ , which is based on cis-eQTLs that maps SNPs to genes up to 1 Mb apart. Chromatin interaction mapping was performed using HiC data (72) of two tissue types (hippocampus and prefrontal cortex) and one cell line (neural progenitor cell) from GSE87112 with a threshold for significant loops of FDR  $< 1 \times 10^{-6}$ . Candidate SNPs were subsequently searched in NHGRI-EBI GWAS catalog (73) to look for previously reported phenotypic associations ( $P < 5 \times 10^{-5}$ ).

### Phenotype-wide association study

We used a general linear model to examine the association of DTI-ALPS index (as dependent variable) with other phenotypes (as independent variable), including traits and diseases, and adjusted for sex, age, and Townsend deprivation index. The results of diseases were presented by  $\beta$  values and its 95% confident intervals, standardized by an increase of one unit in the DTI-ALPS index. The results of traits were presented by Z scores. If the result were a categorical variable, we used the first type of the variable as a reference. The  $P$  values of PheWAS were considered significant at  $P < 2.07 \times 10^{-4}$  adjusting for 241 traits and  $P < 8.00 \times 10^{-5}$  adjusting for 635 diseases using Bonferroni correction.

### Mendelian randomization and mediation analysis

We used bidirectional Mendelian randomization to estimate the causal relationship between DTI-ALPS index with stroke and obesity-related indicators. Our stroke GWAS data are derived from findings of Mishra *et al.* (74), which are the most comprehensive and up-to-date results available. To ensure consistency in selecting obesity-related GWAS IDs, we relied on data from the UK Biobank provided by the Integrative Epidemiology Unit website, except for waist-to-hip ratio (table S10). Despite some overlap between the GWAS samples of ALPS and obesity, the obesity GWAS sample size was tenfold larger, thus enabling us to conduct a two-sample Mendelian randomization analysis.

Bidirectional Mendelian randomizations were conducted using the R package TwoSampleMR (<https://mrcieu.github.io/TwoSampleMR/>). We used the inverse-variance weighted (IVW) model as our main analysis, as well as four other models, namely, Mendelian randomization Egger, weighted median, simple median, and weighted mode as sensitivity analyses. To determine the potential influence of outliers, we applied the Mendelian randomization Pleiotropy RESidual Sum and Outlier (MR-PRESSO) approach. Because of the limited number of variants that passed the genome-wide significance threshold, we selected the genetic variants associated with DTI-ALPS index as instrumental variables based on a  $P < 5 \times 10^{-6}$  threshold. Then, we removed variants in LD using default settings ( $r^2 > 0.001$ , kb  $< 10,000$ ) to ensure independence among the variants. We considered results with  $P < 0.05$  to be statistically significant.

We calculated the mediation effect analysis using  $\beta$  and se values from the results of Mendelian randomization analysis. The indirect effect was calculated as  $\beta_1 \times \beta_2$ , with significance of indirect effects according to the  $t$  test. Mediation proportions were calculated as the ratio of indirect effects to  $\beta_3$ .

### Supplementary Materials

The PDF file includes:

Figs. S1 to S7

Tables S1 to S10

Legends for tables S11 to S17

Other Supplementary Material for this manuscript includes the following:

Tables S11 to S17

### REFERENCES AND NOTES

- J. J. Iliff, M. Wang, Y. Liao, B. A. Plogg, W. Peng, G. A. Gunderson, H. Benveniste, G. E. Vates, R. Deane, S. A. Goldman, E. A. Nagelhus, M. Nedergaard, A paravascular pathway facilitates CSF flow through the brain parenchyma and the clearance of interstitial solutes, including amyloid  $\beta$ . *Sci. Transl. Med.* **4**, 147ra111 (2012).
- B. T. Kress, J. J. Iliff, M. Xia, M. Wang, H. S. Wei, D. Zeppenfeld, L. Xie, H. Kang, Q. Xu, J. A. Liew, B. A. Plogg, F. Ding, R. Deane, M. Nedergaard, Impairment of paravascular clearance pathways in the aging brain. *Ann. Neurol.* **76**, 845–861 (2014).
- L. M. Hablitz, V. Plá, M. Giannetto, H. S. Vinitsky, F. F. Stæger, T. Metcalfe, R. Nguyen, A. Bernais, M. Nedergaard, Circadian control of brain glymphatic and lymphatic fluid flow. *Nat. Commun.* **11**, 4411 (2020).
- B. C. Reeves, J. K. Karimy, A. J. Kundishora, H. Mestre, H. M. Cerci, C. Matouk, S. L. Alper, I. Lundgaard, M. Nedergaard, K. T. Kahle, Glymphatic system impairment in Alzheimer's disease and idiopathic normal pressure hydrocephalus. *Trends Mol. Med.* **26**, 285–295 (2020).
- J. M. Tarasoff-Conway, R. O. Carare, R. S. Osorio, L. Glodzik, T. Butler, E. Fieremans, L. Axel, H. Rusinek, C. Nicholson, B. V. Zlokovic, B. Frangione, K. Blennow, J. Ménard, H. Zetterberg, T. Wisniewski, M. J. de Leon, Clearance systems in the brain—implications for Alzheimer disease. *Nat. Rev. Neurol.* **11**, 457–470 (2015).
- J. L. Hsu, Y. C. Wei, C. H. Toh, I. T. Hsiao, K. J. Lin, T. C. Chen, Y. M. F. Liao, L. S. Ro, Magnetic resonance images implicate that glymphatic alterations mediate cognitive dysfunction in Alzheimer disease. *Ann. Neurol.* **93**, 164–174 (2023).
- K. Kamagata, C. Andica, K. Takabayashi, Y. Saito, T. Taoka, H. Nozaki, J. Kikuta, S. Fujita, A. Hagiwara, K. Kamiya, A. Wada, T. Akashi, K. Sano, M. Nishizawa, M. Hori, S. Naganawa, S. Aoki, Association of MRI indices of glymphatic system with amyloid deposition and cognition in mild cognitive impairment and Alzheimer disease. *Neurology* **99**, e2648–e2660 (2022).
- W. Zhang, Y. Zhou, J. Wang, X. Gong, Z. Chen, X. Zhang, J. Cai, S. Chen, L. Fang, J. Sun, M. Lou, Glymphatic clearance function in patients with cerebral small vessel disease. *Neuroimage* **238**, 118257 (2021).
- Y. Tian, X. Cai, Y. Zhou, A. Jin, S. Wang, Y. Yang, L. Mei, J. Jing, S. Li, X. Meng, T. Wei, T. Liu, Y. Wang, Y. Pan, Y. Wang, Impaired glymphatic system as evidenced by low diffusivity along perivascular spaces is associated with cerebral small vessel disease: A population-based study. *Stroke Vasc. Neurol.* **8**, 413–423 (2023).
- Y. Qin, X. Li, Y. Qiao, H. Zou, Y. Qian, X. Li, Y. Zhu, W. Huo, L. Wang, M. Zhang, DTI-ALPS: An MR biomarker for motor dysfunction in patients with subacute ischemic stroke. *Front. Neurosci.* **17**, 1132393 (2023).
- Y. Tomizawa, A. Hagiwara, Y. Hoshino, M. Nakaya, K. Kamagata, D. Cossu, K. Yokoyama, S. Aoki, N. Hattori, The glymphatic system as a potential biomarker and therapeutic target in secondary progressive multiple sclerosis. *Mult. Scler. Relat. Disord.* **83**, 105437 (2024).
- M. G. Dupreron, M. J. Knol, Q. Le Grand, T. E. Evans, A. Mishra, A. Tsuchida, G. Roshchupkin, T. Konuma, D. A. Tréguoët, J. R. Romero, S. Frenzel, M. Luciano, E. Hofer, M. Bourgey, N. D. Dueker, P. Delgado, S. Hilal, R. M. Tankard, F. Dubost, J. Shin, Y. Saba, N. J. Armstrong, C. Bordes, M. E. Bastin, A. Beiser, H. Brodaty, R. Bülow, C. Carrera, C. Chen, C. Y. Cheng, I. J. Deary, P. G. Gangpawar, J. J. Himali, J. Jiang, T. Kawaguchi, S. Li, M. Macallì, P. Marquis, Z. Morris, S. Muñoz Maniega, S. Miyamoto, M. Okawa, M. Paradise, P. Parva, T. Rundek, M. Sargurupremraj, S. Schilling, K. Setoh, O. Soukarieh, Y. Tabara, A. Teumer, A. Thalamuthu, J. N. Troller, M. C. Valdés Hernández, M. W. Vernooij, U. Völker, K. Wittfeld, T. Y. Wong, M. J. Wright, J. Zhang, W. Zhao, Y. C. Zhu, H. Schmidt, P. S. Sachdev, W. Wen, K. Yoshida, A. Joutel, C. L. Satizabal, R. L. Sacco, G. Bourque, M. Lathrop, T. Paus, I. Fernández-Cadenas, Q. Yang, B. Mazoyer, P. Boutinaud, Y. Okada, H. J. Grabe, K. A. Mather, R. Schmidt, M. Joliot, M. A. Ikram, F. Matsuda, C. Tzourio, J. M. Wardlaw, S. Seshadri, H. H. Adams, S. Debetto, Genomics of perivascular space burden unravels early mechanisms of cerebral small vessel disease. *Nat. Med.* **29**, 950–962 (2023).
- C. H. Wu, F. C. Chang, Y. F. Wang, J. F. Lin, H. M. Wu, L. H. Pan, S. J. Wang, S. P. Chen, Impaired glymphatic and meningeal lymphatic functions in patients with chronic migraine. *Ann. Neurol.* **95**, 583–595 (2024).
- X. Zhang, W. Wang, X. Bai, X. Zhang, Z. Yuan, B. Jiao, Y. Zhang, Z. Li, P. Zhang, H. Tang, Y. Zhang, X. Yu, R. Bai, Y. Wang, B. Sui, Increased glymphatic system activity in migraine chronification by diffusion tensor image analysis along the perivascular space. *J. Headache Pain* **24**, 147 (2023).
- D. A. Lee, H. J. Lee, K. M. Park, Normal glymphatic system function in patients with migraine: A pilot study. *Headache* **62**, 718–725 (2022).

16. B. K. Bulik-Sullivan, P. R. Loh, H. K. Finucane, S. Ripke, J. Yang, N. Patterson, M. J. Daly, A. L. Price, B. M. Neale, LD score regression distinguishes confounding from polygenicity in genome-wide association studies. *Nat. Genet.* **47**, 291–295 (2015).
17. E. M. Stauffer, R. A. I. Bethlehem, L. Dorfschmidt, H. Won, V. Warrier, E. T. Bullmore, The genetic relationships between brain structure and schizophrenia. *Nat. Commun.* **14**, 7820 (2023).
18. R. R. Fagan, P. J. Kearney, C. G. Sweeney, D. Luethi, F. E. S. Uiterkamp, K. Schicker, B. S. Alejandro, L. C. O'Connor, H. H. Sitte, H. E. Melikian, Dopamine transporter trafficking and RIT2 GTPase: Mechanism of action and in vivo impact. *J. Biol. Chem.* **295**, 5229–5244 (2020).
19. J. F. Krey, R. E. Dolmetsch, Molecular mechanisms of autism: A possible role for Ca<sup>2+</sup> signaling. *Curr. Opin. Neurobiol.* **17**, 112–119 (2007).
20. J. Egawa, Y. Watanabe, A. Sugimoto, A. Nunokawa, M. Shibuya, H. Igeta, E. Inoue, S. Hoya, N. Orime, T. Hayashi, T. Sugiyama, T. Someya, Whole-exome sequencing in a family with a monozygotic twin pair concordant for autism spectrum disorder and a follow-up study. *Psychiatry Res.* **229**, 599–601 (2015).
21. A. T. Lu, E. Hannon, M. E. Levine, E. M. Crimmins, K. Lunnon, J. Mill, D. H. Geschwind, S. Horvath, Genetic architecture of epigenetic and neuronal ageing rates in human brain regions. *Nat. Commun.* **8**, 15353 (2017).
22. A. A. Papadopoulou, S. A. Müller, T. Mentrup, M. D. Shmueli, J. Niemeyer, M. Haug-Kröper, J. von Blume, A. Mayerhofer, R. Feederle, B. Schröder, S. F. Lichtenhaller, R. Flührer, Signal peptide peptidase-like 2c impairs vesicular transport and cleaves SNARE proteins. *EMBO Rep.* **20**, e46451 (2019).
23. L. He, Y. Loika, Y. Park, D. A. Bennett, M. Kellis, A. M. Kulminski, Exome-wide age-of-onset analysis reveals exonic variants in ERN1 and SPPL2C associated with Alzheimer's disease. *Transl. Psychiatry* **11**, 146 (2021).
24. S. Da Mesquita, A. Louveau, A. Vaccari, I. Smirnov, R. C. Cornelison, K. M. Kingsmore, C. Contarino, S. Onengut-Gumuscu, E. Farber, D. Raper, K. E. Viar, R. D. Powell, W. Baker, N. Dabhi, R. Bai, R. Cao, S. Hu, S. S. Rich, J. M. Munson, M. B. Lopes, C. C. Overall, S. T. Acton, J. Kipnis, Functional aspects of meningeal lymphatics in ageing and Alzheimer's disease. *Nature* **560**, 185–191 (2018).
25. I. F. Harrison, O. Ismail, A. Machhada, N. Colgan, Y. Ohene, P. Nahavandi, Z. Ahmed, A. Fisher, S. Meftah, T. K. Murray, O. P. Ottersen, E. A. Nagelhus, M. J. O'Neill, J. A. Wells, M. F. Lythgoe, Impaired glymphatic function and clearance of tau in an Alzheimer's disease model. *Brain* **143**, 2576–2593 (2020).
26. W. Zou, T. Pu, W. Feng, M. Lu, Y. Zheng, R. Du, M. Xiao, G. Hu, Blocking meningeal lymphatic drainage aggravates Parkinson's disease-like pathology in mice overexpressing mutated α-synuclein. *Transl. Neurodegener.* **8**, 7 (2019).
27. T. Taoka, Y. Masutani, H. Kawai, T. Nakane, K. Matsuo, F. Yasuno, T. Kishimoto, S. Naganawa, Evaluation of glymphatic system activity with the diffusion MR technique: Diffusion tensor image analysis along the perivascular space (DTI-ALPS) in Alzheimer's disease cases. *Jpn. J. Radiol.* **35**, 172–178 (2017).
28. H. I. Chang, C. W. Huang, S. W. Hsu, S. H. Huang, K. J. Lin, T. Y. Ho, M. C. Ma, W. C. Hsiao, C. C. Chang, Gray matter reserve determines glymphatic system function in young-onset Alzheimer's disease: Evidenced by DTI-ALPS and compared with age-matched controls. *Psychiatry Clin. Neurosci.* **77**, 401–409 (2023).
29. C. D. McKnight, P. Trujillo, A. M. Lopez, K. Petersen, C. Considine, Y. C. Lin, Y. Yan, H. Kang, M. J. Donahue, D. O. Claassen, Diffusion along perivascular spaces reveals evidence supportive of glymphatic function impairment in Parkinson disease. *Parkinsonism Relat. Disord.* **89**, 98–104 (2021).
30. Y. Qin, R. He, J. Chen, X. Zhou, X. Zhou, Z. Liu, Q. Xu, J. F. Guo, X. X. Yan, N. Jiang, W. Liao, T. Taoka, D. Wang, B. Tang, Neuroimaging uncovers distinct relationships of glymphatic dysfunction and motor symptoms in Parkinson's disease. *J. Neurol.* **270**, 2649–2658 (2023).
31. S. Dreha-Kulaczewski, A. A. Joseph, K. D. Merboldt, H. C. Ludwig, J. Gärtner, J. Frahm, Inspiration is the major regulator of human CSF flow. *J. Neurosci.* **35**, 2485–2491 (2015).
32. H. Mestre, J. Tithof, T. Du, W. Song, W. Peng, A. M. Sweeney, G. Olveda, J. H. Thomas, M. Nedergaard, D. H. Kelley, Flow of cerebrospinal fluid is driven by arterial pulsations and is reduced in hypertension. *Nat. Commun.* **9**, 4878 (2018).
33. J. J. Iliff, M. Wang, D. M. Zeppenfeld, A. Venkataraman, B. A. Plog, Y. Liao, R. Deane, M. Nedergaard, Cerebral arterial pulsation drives paravascular CSF-interstitial fluid exchange in the murine brain. *J. Neurosci.* **33**, 18190–18199 (2013).
34. R. T. Kedarasetti, P. J. Drew, F. Costanzo, Arterial pulsations drive oscillatory flow of CSF but not directional pumping. *Sci. Rep.* **10**, 10102 (2020).
35. Y. Liu, P. P. Hu, S. Zhai, W. X. Feng, R. Zhang, Q. Li, C. Marshall, M. Xiao, T. Wu, Aquaporin 4 deficiency eliminates the beneficial effects of voluntary exercise in a mouse model of Alzheimer's disease. *Neural Regen. Res.* **17**, 2079–2088 (2022).
36. X. F. He, D. X. Liu, Q. Zhang, F. Y. Liang, G. Y. Dai, J. S. Zeng, Z. Pei, G. Q. Xu, Y. Lan, Voluntary exercise promotes glymphatic clearance of amyloid beta and reduces the activation of astrocytes and microglia in aged mice. *Front. Mol. Neurosci.* **10**, 144 (2017).
37. L. Xie, H. Kang, Q. Xu, M. J. Chen, Y. Liao, M. Thiagarajan, J. O'Donnell, D. J. Christensen, C. Nicholson, J. J. Iliff, T. Takano, R. Deane, M. Nedergaard, Sleep drives metabolite clearance from the adult brain. *Science* **342**, 373–377 (2013).
38. A. Miao, T. Luo, B. Hsieh, C. J. Edge, M. Gridley, R. T. C. Wong, T. G. Constandinou, W. Wisden, N. P. Franks, Brain clearance is reduced during sleep and anesthesia. *Nat. Neurosci.* **27**, 1046–1050 (2024).
39. B. Ozturk, S. Koundal, E. Al Bizri, X. Chen, Z. Gursky, F. Dai, A. Lim, P. Heerdjt, J. Kipnis, A. Tannenbaum, H. Lee, H. Benveniste, Continuous positive airway pressure increases CSF flow and glymphatic transport. *JCI Insight* **8**, e170270 (2023).
40. L. J. H. Rasmussen, A. Caspi, A. Ambler, J. M. Broadbent, H. J. Cohen, T. d'Arbeloff, M. Elliott, R. J. Hancock, H. Harrington, S. Hogan, R. Houts, D. Ireland, A. R. Knott, K. Meredith-Jones, M. C. Morey, L. Morrison, R. Poulton, S. Ramrakha, L. Richmond-Rakerd, M. L. Sison, K. Sneddon, W. M. Thomson, A. R. Hariri, T. E. Moffitt, Association of neurocognitive and physical function with gait speed in midlife. *JAMA Netw. Open* **2**, e1913123 (2019).
41. K. Vladimir, M. M. Perišić, M. Štorga, A. Mostashari, R. Khanin, Epigenetics insights from perceived facial aging. *Clin. Epigenetics* **15**, 176 (2023).
42. R. Daviet, G. Aydogan, K. Jagannathan, N. Spilka, P. D. Koellinger, H. R. Kranzler, G. Nave, R. R. Wetherill, Associations between alcohol consumption and gray and white matter volumes in the UK Biobank. *Nat. Commun.* **13**, 1175 (2022).
43. C. Andica, K. Kamagata, K. Takabayashi, J. Kikuta, H. Kaga, Y. Someya, Y. Tamura, R. Kawamori, H. Watada, T. Taoka, S. Naganawa, S. Aoki, Neuroimaging findings related to glymphatic system alterations in older adults with metabolic syndrome. *Neurobiol. Dis.* **177**, 105990 (2023).
44. C. H. Toh, T. Y. Siow, Glymphatic dysfunction in patients with ischemic stroke. *Front. Aging Neurosci.* **13**, 756249 (2021).
45. V. Kiviniemi, X. Wang, V. Korhonen, T. Keinänen, T. Tuovinen, J. Autio, P. LeVan, S. Keilholz, Y. F. Zang, J. Hennig, M. Nedergaard, Ultra-fast magnetic resonance encephalography of physiological brain activity – Glymphatic pulsation mechanisms? *J. Cereb. Blood Flow Metab.* **36**, 1033–1045 (2016).
46. M. Olaithre, R. S. Bucks, D. R. Hillman, P. R. Eastwood, Cognitive deficits in obstructive sleep apnea: Insights from a meta-review and comparison with deficits observed in COPD, insomnia, and sleep deprivation. *Sleep Med. Rev.* **38**, 39–49 (2018).
47. G. Li, J. Liu, M. Guo, Y. Gu, Y. Guan, Q. Shao, W. Ma, X. Ji, Chronic hypoxia leads to cognitive impairment by promoting HIF-2α-mediated ceramide catabolism and alpha-synuclein hyperphosphorylation. *Cell Death Discov.* **8**, 473 (2022).
48. Q. Aziz, D. G. Thompson, Brain-gut axis in health and disease. *Gastroenterology* **114**, 559–578 (1998).
49. T. G. Dinan, J. F. Cryan, Gut-brain axis in 2016: Brain-gut-microbiota axis – Mood, metabolism and behaviour. *Nat. Rev. Gastroenterol. Hepatol.* **14**, 69–70 (2017).
50. A. Gupta, V. Osadchy, E. A. Mayer, Brain-gut-microbiome interactions in obesity and food addiction. *Nat. Rev. Gastroenterol. Hepatol.* **17**, 655–672 (2020).
51. Y. Yuan, X. Wang, S. Huang, H. Wang, G. Shen, Low-level inflammation, immunity, and brain-gut axis in IBS: Unraveling the complex relationships. *Gut Microbes* **15**, 2263209 (2023).
52. Y. C. Wei, C. H. Hsu, W. Y. Huang, C. Lin, C. K. Chen, Y. L. Chen, P. Y. Chen, Y. C. Shyu, C. P. Lin, Vascular risk factors and astrocytic marker for the glymphatic system activity. *Radiol. Med.* **128**, 1148–1161 (2023).
53. Y. Tian, M. Zhao, Y. Chen, M. Yang, Y. Wang, The underlying role of the glymphatic system and meningeal lymphatic vessels in cerebral small vessel disease. *Biomolecules* **12**, 748 (2022).
54. H. Mestre, Y. Mori, M. Nedergaard, The brain's glymphatic system: Current controversies. *Trends Neurosci.* **43**, 458–466 (2020).
55. K. Ishida, K. Yamada, R. Nishiyama, T. Hashimoto, I. Nishida, Y. Abe, M. Yasui, T. Iwatubo, Glymphatic system clears extracellular tau and protects from tau aggregation and neurodegeneration. *J. Exp. Med.* **219**, e20211275 (2022).
56. D. Jiang, L. Liu, Y. Kong, Z. Chen, P. Rosa-Neto, K. Chen, L. Ren, M. Chu, L. Wu, Regional glymphatic abnormality in behavioral variant frontotemporal dementia. *Ann. Neurol.* **94**, 442–456 (2023).
57. Z. Fu, A. Sajad, S. P. Errington, J. D. Schall, U. Rutishauser, Neurophysiological mechanisms of error monitoring in human and non-human primates. *Nat. Rev. Neurosci.* **24**, 153–172 (2023).
58. D. Badre, D. E. Nee, Frontal cortex and the hierarchical control of behavior. *Trends Cogn. Sci.* **22**, 170–188 (2018).
59. M. Muthuraman, M. Palotai, B. Jávor-Duray, A. Kelemen, N. Koirala, L. Halász, L. Erőss, G. Fekete, L. Bognár, G. Deuschl, G. Tamás, Frequency-specific network activity predicts bradykinesia severity in Parkinson's disease. *NeuroImage Clin.* **32**, 102857 (2021).
60. K. George, J. M. Das, in StatPearls. (StatPearls Publishing LLC, Treasure Island (FL) ineligible companies. Disclosure: Joe Das declares no relevant financial relationships with ineligible companies., 2024).
61. A. M. Wright, Y. C. Wu, L. Feng, Q. Wen, Diffusion magnetic resonance imaging of cerebrospinal fluid dynamics: Current techniques and future advancements. *NMR Biomed.* **37**, e5162 (2024).
62. T. Taoka, R. Ito, R. Nakamichi, T. Nakane, H. Kawai, S. Naganawa, Diffusion tensor image analysis along the perivascular space (DTI-ALPS): Revisiting the meaning and significance of the method. *Magn. Reson. Med. Sci.* **23**, 268–290 (2024).

63. F. Alfaro-Almagro, M. Jenkinson, N. K. Bangerter, J. L. R. Andersson, L. Griffanti, G. Douaud, S. N. Sotiropoulos, S. Jbabdi, M. Hernandez-Fernandez, E. Vallee, D. Vidaurre, M. Webster, P. McCarthy, C. Rorden, A. Daducci, D. C. Alexander, H. Zhang, I. Dragou, P. M. Matthews, K. L. Miller, S. M. Smith, Image processing and quality control for the first 10,000 brain imaging datasets from UK Biobank. *Neuroimage* **166**, 400–424 (2018).
64. B. B. Avants, C. L. Epstein, M. Grossman, J. C. Gee, Symmetric diffeomorphic image registration with cross-correlation: Evaluating automated labeling of elderly and neurodegenerative brain. *Med. Image Anal.* **12**, 26–41 (2008).
65. C. Bycroft, C. Freeman, D. Petkova, G. Band, L. T. Elliott, K. Sharp, A. Motyer, D. Vukcevic, O. Delaneau, J. O'Connell, A. Cortes, S. Welsh, A. Young, M. Effingham, G. McVean, S. Leslie, N. Allen, P. Donnelly, J. Marchini, The UK Biobank resource with deep phenotyping and genomic data. *Nature* **562**, 203–209 (2018).
66. X. Hao, Z. Shao, N. Zhang, M. Jiang, X. Cao, S. Li, Y. Guan, C. Wang, Integrative genome-wide analyses identify novel loci associated with kidney stones and provide insights into its genetic architecture. *Nat. Commun.* **14**, 7498 (2023).
67. C. C. Chang, C. C. Chow, L. C. Tellier, S. Vattikuti, S. M. Purcell, J. J. Lee, Second-generation PLINK: Rising to the challenge of larger and richer datasets. *GigaScience* **4**, 7 (2015).
68. H. K. Finucane, B. Bulik-Sullivan, A. Gusev, G. Trynka, Y. Reshef, P.-R. Loh, V. Anttila, H. Xu, C. Zang, K. Farh, Partitioning heritability by functional annotation using genome-wide association summary statistics. *Nat. Genet.* **47**, 1228–1235 (2015).
69. K. Watanabe, E. Taskesen, A. van Bochoven, D. Posthuma, Functional mapping and annotation of genetic associations with FUMA. *Nat. Commun.* **8**, 1826 (2017).
70. K. Wang, M. Li, H. Hakonarson, ANNOVAR: Functional annotation of genetic variants from high-throughput sequencing data. *Nucleic Acids Res.* **38**, e164 (2010).
71. GTEx Consortium, Human genomics. The genotype-tissue expression (GTEx) pilot analysis: Multitissue gene regulation in humans. *Science* **348**, 648–660 (2015).
72. A. D. Schmitt, M. Hu, I. Jung, Z. Xu, Y. Qiu, C. L. Tan, Y. Li, S. Lin, Y. Lin, C. L. Barr, B. Ren, A compendium of chromatin contact maps reveals spatially active regions in the human genome. *Cell Rep.* **17**, 2042–2059 (2016).
73. J. MacArthur, E. Bowler, M. Cerezo, L. Gil, P. Hall, E. Hastings, H. Junkins, A. McMahon, A. Milano, J. Morales, Z. M. Pendlington, D. Welter, T. Burdett, L. Hindorff, P. Flück, F. Cunningham, H. Parkinson, The new NHGRI-EBI Catalog of published genome-wide association studies (GWAS Catalog). *Nucleic Acids Res.* **45**, D896–d901 (2017).
74. A. Mishra, R. Malik, T. Hachiya, T. Jürgenson, S. Namba, D. C. Posner, F. K. Kamanu, M. Koido, Q. Le Grand, M. Shi, Y. He, M. K. Georgakis, I. Caro, K. Krebs, Y. C. Liaw, F. C. Vaura, K. Lin, B. S. Winsvold, V. Srivivasasainagendra, L. Parodi, H. J. Bae, G. Chauhan, M. R. Chong, L. Tomppo, R. Akinyemi, G. V. Roschupkin, N. Habib, Y. H. Jee, J. Q. Thomassen, V. Abedi, J. Cárcel-Márquez, M. Nygaard, H. L. Leonard, C. Yang, E. Yonova-Doing, M. J. Knol, A. J. Lewis, R. L. Judy, T. Ago, P. Amouyel, N. D. Armstrong, M. K. Bakker, T. M. Bartz, D. A. Bennett, J. C. Bis, C. Bordes, S. Børte, A. Cain, P. M. Ridker, K. Cho, Z. Chen, C. Cruchaga, J. W. Cole, P. L. de Jager, R. de Cid, M. Endres, L. E. Ferreira, M. I. Geerlings, N. C. Gasca, V. Gudnason, J. Hata, J. He, A. K. Heath, Y. L. Ho, A. S. Havulinna, J. C. Hopewell, H. I. Hyacinth, M. Inouye, M. A. Jacob, C. E. Jeon, C. Jern, M. Kamouchi, K. L. Keene, T. Kitazono, S. J. Kittner, T. Konuma, A. Kumar, P. Lacaze, L. J. Launer, K. J. Lee, K. Lepik, J. Li, L. Li, A. Manichaikul, H. S. Markus, N. A. Marston, T. Meitinger, B. D. Mitchell, F. A. Montellano, T. Morisaki, T. H. Mosley, M. A. Nalls, B. G. Nordestgaard, M. J. O'Donnell, Y. Okada, N. C. Onland-Moret, B. Ovbiegele, A. Peters, B. M. Psaty, S. S. Rich, J. Rosand, M. S. Sabatine, R. L. Sacco, D. Saleheen, E. C. Sandset, V. Salomaa, M. Sargurupremraj, M. Sasaki, C. L. Satizabal, C. O. Schmidt, A. Shimizu, N. L. Smith, K. L. Sloane, Y. Sutoh, Y. V. Sun, K. Tanno, S. Tiedt, T. Tatlisumak, N. P. Torres-Aguila, H. K. Tiwari, D. A. Trégoüët, S. Trompet, A. M. Tuladhar, A. Tybjærg-Hansen, M. van Vugt, R. Vibo, S. S. Verma, K. L. Wiggins, P. Wennberg, D. Woo, P. W. F. Wilson, H. Xu, Q. Yang, K. Yoon, I. Y. Millwood, C. Gieger, T. Niinomiya, H. J. Grabe, J. W. Jukema, I. L. Rissanen, D. Strbian, Y. J. Kim, P. H. Chen, E. Mayerhofer, J. M. M. Howson, M. R. Irvin, H. Adams, S. Wassertheil-Smoller, K. Christensen, M. A. Ikram, T. Rundek, B. B. Worrall, G. M. Lathrop, M. Riaz, E. M. Simonsick, J. Körv, P. H. C. França, R. Zand, K. Prasad, R. Frikkie-Schmidt, F. E. de Leeuw, T. Liman, K. G. Haeusler, Y. M. Ruigrok, P. U. Heuschmann, W. T. Longstreth, K. J. Jung, L. Bastarache, G. Paré, S. M. Damrauer, D. I. Chasman, J. I. Rotter, C. D. Anderson, J. A. Zwart, T. J. Niiranen, M. Fornage, Y. P. Liaw, S. Seshadri, I. Fernández-Cadenas, R. G. Walters, C. T. Ruff, M. O. Owolabi, J. E. Huffman, L. Milani, Y. Kamatani, M. Dichgans, S. Debette, Stroke genetics informs drug discovery and risk prediction across ancestries. *Nature* **611**, 115–123 (2022).

**Acknowledgments:** We thank the UK Biobank participants. We conducted this research under the UK Biobank application no. 90311. We thank P. Cumming of the Bern University for critical reading of the manuscript. The computation is completed in the HPC Platform of Huazhong University of Science and Technology. **Funding:** The National Key R&D Program of China (program ID: 2021YFC2502200, recipient: M.W.), the National Natural Science Foundation of China (program ID: 82271355, recipient: M.W.; program ID: 32470658, recipient: X.H.), and Hubei Provincial Natural Science Foundation (program ID: 2022CFA097, recipient: M.W.).

**Author contributions:** Conceptualization: M.W., X.H., L.R., and Y.F. Methodology: M.W., X.H., L.R., and Y.F. Investigation: M.W., X.H., L.R., Y.F., and C.C. Formal analysis: M.W., X.H., L.R., Y.F., and C.C. Software: X.H., L.R., Y.F., and Z.S. Visualization: X.H., L.R., Y.F., C.C., Y.H., Z.S., and Y.K. Resources: M.W., X.H., Y.F., and Z.S. Data curation: M.W., X.H., Y.F., and Z.S. Validation: M.W., X.H., and Y.F. Funding acquisition: M.W., X.H., and W.W. Project administration: M.W., X.H., Y.F., Z.S., and W.W. Supervision: X.H., Y.F., H.H., S.X., and X.L. Writing—original draft: M.W., X.H., L.R., Y.F., C.C., and Y.H. Writing—review and editing: M.W., X.H., Y.F., and Z.S. **Competing interests:** The authors declare that they have no competing interests. **Data and materials availability:** All imaging, phenotypes and genetics data are available from the UK Biobank via standard data access procedure (see <http://ukbiobank.ac.uk/register-apply>). The function annotation of all SNPs, detailed results of PheWAS, and data processing of UK Biobank have been disposed as tables S11 to S17 and deposited on figshare (see <https://doi.org/10.6084/m9.figshare.27997871.v1>). Summary statistics of the DTI-ALPS index in this study are available in the GWAS catalog (GCST90455543-GCST90455546). All data needed to evaluate the conclusions in the paper are present in the paper and/or the Supplementary Materials.

Submitted 2 July 2024

Accepted 16 December 2024

Published 17 January 2025

10.1126/sciadv.adr4606